

Impact of Wind Direction, Wind Speed, and Particle Characteristics on the Collection Efficiency of the Double Fence Intercomparison Reference

JULIE M. THÉRIAULT

Department of Earth and Atmospheric Sciences, Université du Québec à Montréal, Montreal, Quebec, Canada

ROY RASMUSSEN

Research Application Laboratory, National Center for Atmospheric Research, Boulder, Colorado*

EDDY PETRO AND JEAN-YVES TRÉPANIER

Department of Mechanical Engineering, École Polytechnique Montréal, Montreal, Quebec, Canada

MATTEO COLLI AND LUCA G. LANZA

Department of Civil, Chemical and Environmental Engineering, University of Genoa, and WMO/CIMO Lead Centre "B. Castelli" on Precipitation Intensity, Genoa, Italy

(Manuscript received 17 December 2014, in final form 15 May 2015)

ABSTRACT

The accurate measurement of snowfall is important in various fields of study such as climate variability, transportation, and water resources. A major concern is that snowfall measurements are difficult and can result in significant errors. For example, collection efficiency of most gauge–shield configurations generally decreases with increasing wind speed. In addition, much scatter is observed for a given wind speed, which is thought to be caused by the type of snowflake. Furthermore, the collection efficiency depends strongly on the reference used to correct the data, which is often the Double Fence Intercomparison Reference (DFIR) recommended by the World Meteorological Organization. The goal of this study is to assess the impact of weather conditions on the collection efficiency of the DFIR. Note that the DFIR is defined as a manual gauge placed in a double fence. In this study, however, only the double fence is being investigated while still being called DFIR. To address this issue, a detailed analysis of the flow field in the vicinity of the DFIR is conducted using computational fluid dynamics. Particle trajectories are obtained to compute the collection efficiency associated with different precipitation types for varying wind speed. The results show that the precipitation reaching the center of the DFIR can exceed 100% of the actual precipitation, and it depends on the snowflake type, wind speed, and direction. Overall, this study contributes to a better understanding of the sources of uncertainty associated with the use of the DFIR as a reference gauge to measure snowfall.

1. Introduction

The measurement of snowfall is important in various fields of study such as climate variability, transportation,

and water resources. Measuring snowfall amount accurately is challenging, however, because of the many sources of uncertainty associated with the weather conditions and technical factors (e.g., Groisman et al. 1991; Groisman and Legates 1994; Yang et al. 1995; Sugiura et al. 2006; Rasmussen et al. 2012). Accumulated snowfall during the cold season has various implications. For example, it is used to study the precipitation variability associated with climate change. Over a seasonal time scale, it affects the amount of water resources during the spring season. Measuring the amount of snowpack is critical to assessing flood

* The National Center for Atmospheric Research is sponsored by the National Science Foundation.

Corresponding author address: Julie M. Thériault, Dept. of Earth and Atmospheric Sciences, Université du Québec à Montréal, P.O. Box 8888, Succursale Centre-Ville, Montreal, QC H3C 3P8, Canada.
E-mail: theriault.julie@uqam.ca

warnings as well. Over a shorter time scale, the amount of snow accumulated during a storm can affect air and ground transportation (e.g., [Rasmussen et al. 2001](#)).

The main problem associated with the measurement of solid precipitation by automatic gauges is the effect of the wind ([Goodison et al. 1998](#)). It is common to observe large differences in the amount of precipitation measured by various gauge–shield configurations located at the same observational site ([Rasmussen et al. 2012](#)). The difference among the different methods to measure snow can be up to 75%. To assess the performance of the different gauge–shield configurations, collection efficiencies are calculated on the basis of the amount of precipitation measured by a reference gauge–shield configuration. In 1985, the World Meteorological Organization (WMO)/Commission for Instruments and Methods of Observation designated the Double Fence Intercomparison Reference (DFIR) as a secondary reference to a bush-shielded Tretyakov gauge to compare with the standard shield for precipitation measurements, which is the bush gauge ([Goodison et al. 1998](#)). For that experiment, a small metal shield called the Tretyakov fence ([Yang et al. 1995](#)) was installed in the center of the DFIR. A study by [Yang \(2014\)](#) showed that the DFIR undercollects precipitation by ~5% with respect to the bush gauge. The Tretyakov shield was recently replaced by a single Alter shield ([Alter 1937](#)), and [Smith \(2009\)](#) studied the performance of this gauge–shield configuration. That gauge–shield configuration (double fence with a Geonor, Inc., gauge placed in a single Alter shield) is currently being used by the WMO Solid Precipitation Intercomparison Experiment (SPICE; [Nitu et al. 2012](#)) as the reference for automated snow gauges. Note that [Rasmussen et al. \(2012\)](#) showed that a Geonor T-200B gauge placed in a DFIR wind fence measures higher snowfall rates in strong wind speed conditions than do other gauge–shield configurations located on the same site. No bush gauge, however, is being tested at that site.

The collection efficiency of all gauge–shield configurations generally decreases with increasing wind speed. This tendency in the collection efficiency has been observed at many WMO sites around the world ([Goodison et al. 1998](#)). This wind-induced error is fundamentally caused by the deformation of the flow in the vicinity of the gauge orifice, which creates an updraft that prevents particles from falling into the gauge (e.g., [Thériault et al. 2012](#); [Rasmussen et al. 2012](#)). The shield around the gauge acts to slow down the wind speed and, in turn, decreases the strength of the updraft upstream of the gauge orifice. This effect generally leads to an increase of the collection efficiency. [Nespor and Sevruk \(1999\)](#) have addressed this issue by simulating raindrop trajectories in the vicinity of a gauge. [Goodison et al. \(1998\)](#)

made initial studies on snowflake trajectories. They showed that the lighter the snowflakes are, the higher is the wind-induced error for two different precipitation gauges (automated tipping-bucket type, or ASTA, and Hellman type).

Despite the decrease in the collection efficiency with increasing wind speed, large scatter in the data is also observed at a given wind speed. This scatter can be due to technical factors that are associated with sensors, wetting, evaporation losses, and turbulent airflows ([Yang et al. 2005](#)). [Thériault et al. \(2012\)](#) showed, using both computational fluid dynamics (CFD) modeling and detailed snowflake-type observations, that the terminal velocity of the precipitation affects the collection efficiency of the gauge. For example, slow-falling snowflakes are generally pushed away from the gauge orifice and are not collected because they tend to follow the streamlines. On the other hand, the fast-falling snowflakes cross the streamlines and will tend to fall inside the gauge, leading to a higher collection efficiency than is associated with slow-falling snowflakes.

Given the large amount of scatter associated with the collection efficiency at a given wind speed, it is critical to identify the sources of uncertainty that affect the automatic measurement of solid precipitation. Furthermore, the performance of a gauge–shield configuration depends on the amount of precipitation measured by the gauge of interest as well as by the one placed in a DFIR. The goal of this study is to investigate the collection efficiency of a Geonor model T200-B gauge installed within the DFIR with respect to wind speed and direction as well as precipitation types. Note that the DFIR was originally defined as a manual gauge placed in an octagonal double fence. Only this double fence is investigated in this study, which configuration will still be called DFIR. This is achieved by using CFD and a Lagrangian model that was specifically developed to track a variety of snowflake types. In particular, the uncertainty associated with the type of snow, the wind speed, and the direction has been investigated. The wind direction with respect to the orientation of the DFIR is taken into account because of the octagonal shape of the fence. The numerical results have been compared with data collected at the Marshall test site that is located near Boulder, Colorado, during the winters of 2012–14 using gauges placed in DFIRs that are oriented differently with respect to north.

The paper is organized as follows: The experimental design is described in [section 2](#). The flow field around the DFIR is analyzed in [section 3](#). The collection efficiency of the DFIR is discussed in [section 4](#). The results are compared with observations in [section 5](#), and [section 6](#) presents the concluding remarks.

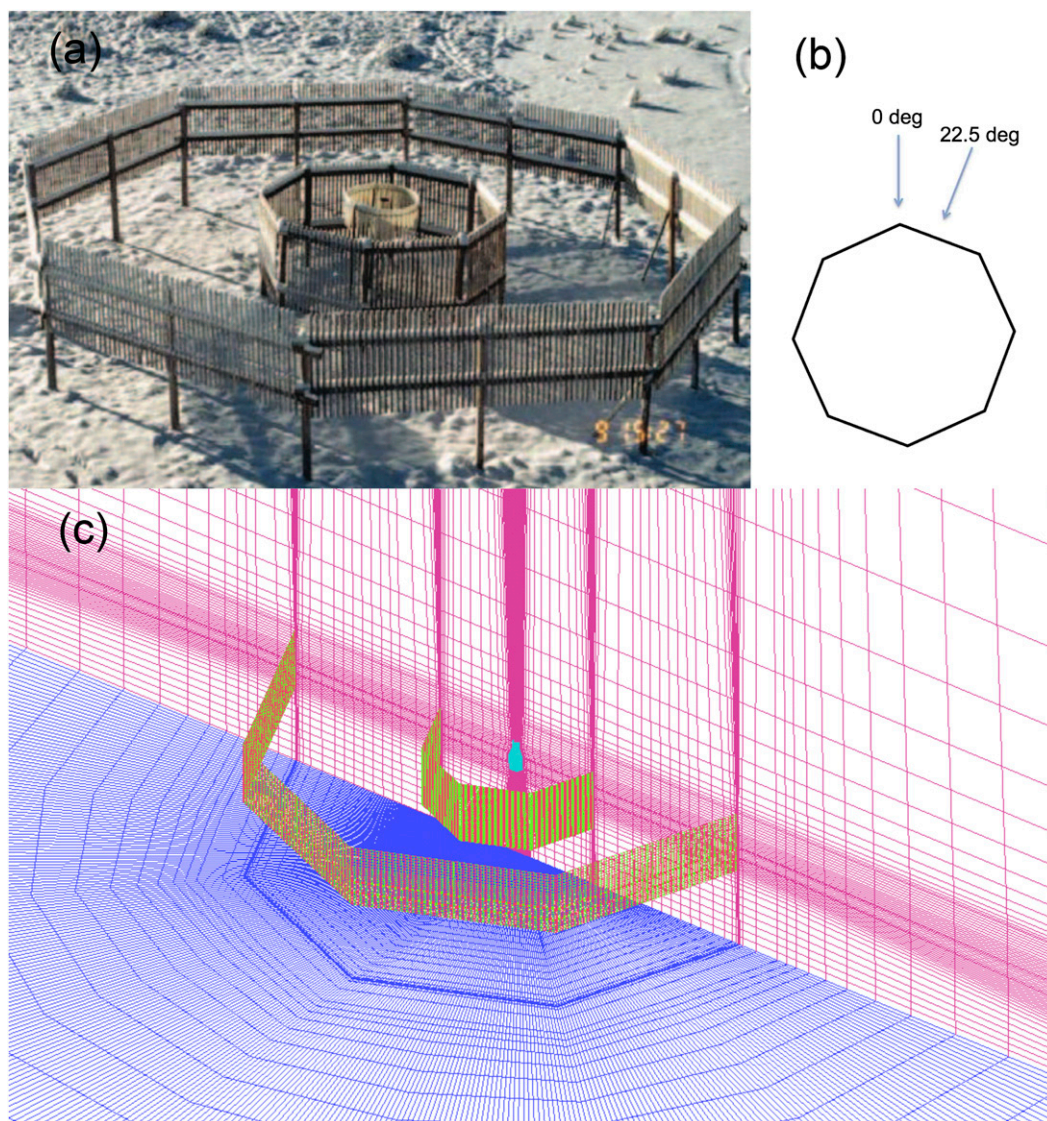


FIG. 1. (a) Picture [taken from [Rasmussen et al. \(2012\)](#)] of a DFIR with a Geonor T-200B gauge inside. In general, this gauge–shield configuration uses a single Alter shield in the inside fence. To focus on the collection efficiency of the DFIR we have omitted the impact of the single Alter shield. (b) The wind directions tested in the numerical simulations. (c) A view of the 0° orientation mesh used for the CFD analysis.

2. Experimental design

To assess the collection efficiency of the DFIR, numerical simulations and a particle trajectory model were used. This method follows that of previous studies conducted by [Nespor and Sevruc \(1999\)](#), [Thériault et al. \(2012\)](#), and [Colli et al. \(2015a,b,c\)](#).

a. Flow-field simulations

The time-averaged flow field near the DFIR was simulated using ANSYS, Inc., “ANSYS Fluent” model,

version 13, and by assuming symmetry in the flow field. The symmetry decision was made to reduce the computing time because, as shown in [Fig. 1a](#), the DFIR is 12 m wide and 3.5 m high. This is at least 6 times as wide as a single Alter shield. Furthermore, the porosity of the DFIR is 50%. Because the DFIR is octagonal, two different DFIR orientations were tested to account for the flow field perpendicular to a side (22.5°) and to a vertex (0°) of the DFIR. These are the two extreme cases associated with an octagonal shape and shown in [Fig. 1b](#). For simplicity and to specifically study the collection

efficiency of the DFIR, the simulations have been conducted without the single Alter shield often placed in the middle of the inner fence. Note that the flow field was also simulated inside the gauge.

Manual hexahedron meshing was created to resolve the airflow near the interface of the fences and the gauge. A total of 3 million mesh points were used for each of the simulated wind directions. Furthermore, the hexahedron mesh was aligned with respect to the wind direction to increase the accuracy of the flow field. A view of the mesh is provided in Fig. 1c. It can be observed that the mesh is denser in regions of interest near the gauge and the fences. The normal thickness of the first cells adjacent to the gauge and shield walls is situated within $30 < y+ < 300$, where $y+$ is the standard nondimensional wall distance used in CFD solutions. All of the boundaries of the perimeter were defined as solid walls except for the inflow and the outflow sides of the box. These boundary conditions allowed an environment around the gauge to be of a sufficient size such that the wind flow was uniform before encountering the gauge–shield configuration.

The flow simulation was performed using the Reynolds-averaged Navier–Stokes equations (RANS) standard $k-\epsilon$ turbulence–dissipation model with scalable wall functions. The flow field was simulated around and in the DFIR as well as inside the gauge. The implicit pressure-based solver was used, together with a second-order upwind scheme. The initialization of the flow field in ANSYS Fluent required several conditions. First, the fluid in the box was defined as air (1 kg m^{-3}). Second, a wind speed value was initialized on the inflow wall. Constant wind speed values with height of $1\text{--}9 \text{ m s}^{-1}$ were tested with increments of 2 m s^{-1} . The assumption of constant wind speed values with height follows Thériault et al. (2012) and more recently Colli et al. (2015a,b). These studies reproduced closely the observed collection efficiency. A varying wind speed with height would probably produce eddies, however, which can lead to some variation in the results. For all of these cases, Fluent was run until it converged to a steady mean $k-\epsilon$ turbulent flow.

b. Snow trajectories

The Lagrangian model used in this study followed Thériault et al. (2012) and Nespor and Sevruck (1999). The flow field obtained with Fluent was used to initialize and simulate the trajectories with the Lagrangian model. The model is briefly summarized below.

The equation determining the particle motion is

$$V_s \rho_s \mathbf{a}_s = -C_d A_s \rho_a \frac{1}{2} (\mathbf{v}_s - \mathbf{v}_a) |\mathbf{v}_s - \mathbf{v}_a| + V_s (\rho_s - \rho_a) \mathbf{g}, \quad (1)$$

TABLE 1. The parameters used in the Lagrangian model and to compute the collection efficiency [Eq. (8)]. The parameters of the terminal velocity are a_T and b_T , the parameters of the density are a_D and b_D , and the parameters of the volume are a_V and b_V . These values are for a snowflake diameter measured in meters.

	$a_T (\text{m}^{1-b_T} \text{s}^{-1})$	b_T	$a_D (\text{kg m}^{-2})$	b_D	a_V	b_V
Dry snow	2.69	0.2	0.017	−1	$\pi/6$	3
Wet snow	5.38	0.2	0.072	−1	$\pi/6$	3

where \mathbf{a}_s is the snowflake acceleration, V_s is the volume of the snowflake, ρ_s is the snow density, ρ_a is the air density, C_d is the drag coefficient [Eq. (7), below], A_s is the cross-sectional area normal to the flow (assumed to be circular), \mathbf{v}_s is the velocity of the snowflake, \mathbf{v}_a is the velocity of the fluid, \mathbf{g} is the gravitational acceleration, and $|\mathbf{v}_s - \mathbf{v}_a|$ is the magnitude of the velocity vector:

$$|\mathbf{v}_s - \mathbf{v}_a| = [(u_s - u_a)^2 + (v_s - v_a)^2 + (w_s - w_a)^2]^{1/2}, \quad (2)$$

where u_x is the velocity component along the x axis, v_x is the velocity component along the y axis, and w_x is the velocity component along the z axis for the snowflake (subscript s) and the environmental air (subscript a). Hence, the components of the acceleration vector are

$$a_x = -\frac{1}{2} C_d A \frac{\rho_a}{V_s \rho_s} (u_s - u_a) |\mathbf{v}_s - \mathbf{v}_a|, \quad (3)$$

$$a_y = -\frac{1}{2} C_d A \frac{\rho_a}{V_s \rho_s} (v_s - v_a) |\mathbf{v}_s - \mathbf{v}_a|, \quad \text{and} \quad (4)$$

$$a_z = -\frac{1}{2} C_d A \frac{\rho_a}{V_s \rho_s} (w_s - w_a) |\mathbf{v}_s - \mathbf{v}_a| + \frac{(\rho_s - \rho_a)}{\rho_s} g. \quad (5)$$

The snowflake is initialized far upstream of the DFIR where the wind speed is not perturbed by the geometry. The initial position of the snowflake depends on the wind speed to minimize the computing time for the trajectories. For example, snowflakes falling in a 9 m s^{-1} flow field are initialized farther upstream than are particles in a 1 m s^{-1} wind field. At that location, the initial particle velocity is assumed to be the terminal velocity (z axis) of the given type and dimension of the snowflake and the horizontal wind speed (x axis). The terminal velocity is

$$v_T(D) = a_T D^{b_T}, \quad (6)$$

where the values are given in Table 1. Because the initial flow is initialized along the y axis, the initial value of the snowflake velocity in the crosswise direction is zero. Given the initial position and velocity of the particle, the acceleration of the particle is computed, and, in turn, the three-dimensional location of the snowflake is known at

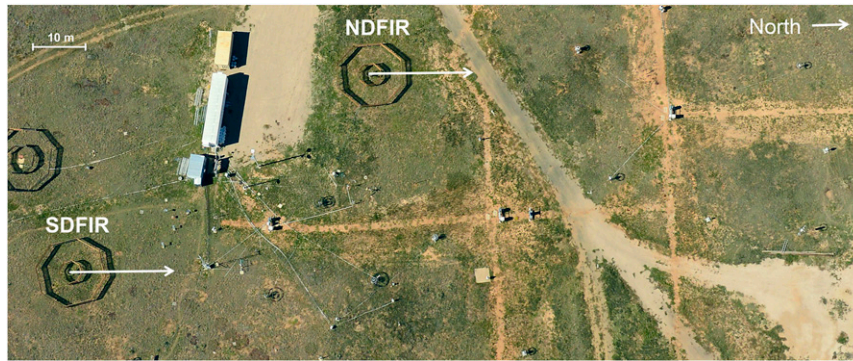


FIG. 2. The location of the two DFIRs used in this study. NDFIR refers to the DFIR located farther north, and the SDFIR refers to the one located to the south of the NDFIR. A northerly wind is associated with a 22.5° wind orientation for the NDFIR and a 0° wind orientation for the SDFIR. Note that the exact orientation of the SDFIR is 8.5° with respect to north.

each time step. The time step was adjusted on the basis of the value of the initial wind speed. As in Nespor and Sevruk (1999), it was set for a $\Delta x = 3$ mm. Hence, it varies from 0.001 to 0.00035 s.

The snowflake categories considered in this study are wet and dry snow. The theoretical values that characterize these precipitation types were used in Thériault et al. (2012) and were obtained from Rasmussen et al. (1999). The differentiation between wet and dry snow is mainly the air temperature but also the particle density, with wet snow typically being more heavily rimed. This aspect is discussed in more detail in section 2d. The drag coefficient used in the simulations in this study is based on the one for ice crystals in a turbulent regime that is described in Khvorostyanov and Curry (2005). The use of this drag-coefficient formulation has been shown by Colli et al. (2015c) to provide superior particle trajectories for simulations past an unshielded Geonor gauge and an Alter-shielded Geonor gauge. The formulation is given as

$$C_D = 12.04\text{Re}^{-0.373}, \quad (7)$$

where Re is the Reynolds number.

c. Calculation of the collection efficiency

The calculation of the collection efficiency requires a few steps. First, the number of snowflakes that fall in the gauge is computed with the trajectory model. The particles are initialized on a horizontal plane upstream of the fences, where their initial positions are evenly spaced ($1\text{ cm} \times 1\text{ cm}$). Second, because snowflakes follow an inverse exponential particle size distribution (Marshall and Palmer 1948), the collection efficiency is calculated for a range of snowflake diameters—0.5, 0.75, 1, 2, 3, 4, 5, 6, 7, 8, 9, 10, 15, and 20 mm—for both wet and

dry snow. Third, because the gauge measures the mass of liquid water and the snow density varies with the size of snow, we consider a mass–diameter factor (volumetric method; Colli et al. 2015b) in the calculation of the collection efficiency. Therefore, the theoretical collection efficiency is defined as

$$\text{CE} = \frac{\int_0^{D_{\max}} A_{\text{inside}}(D)\rho(D)V(D)\exp(-\lambda D)dD}{\int_0^{D_{\max}} A_{\text{gauge}}\rho(D)V(D)\exp(-\lambda D)dD}, \quad (8)$$

where D_{\max} is the maximum size of snow, A_{inside} is the effective collecting area that is associated with the number of snowflakes falling inside the gauge, A_{gauge} is the area that is associated with the number of snowflakes falling inside the gauge in an undisturbed flow, λ is the slope parameter of the particle size distribution, $\rho(D)$ is the density of the snowflake type (defined as $a_D D^{b_D}$), and $V(D)$ is the volume of the particles (defined as $a_V D^{b_V}$). The values are given in Table 1.

These steps are repeated for five initial wind speeds: 1, 3, 5, 7, and 9 m s^{-1} . The slope of the size distribution used was 1 mm^{-1} as based on Houze et al. (1979) who observed the snow size distribution in different atmospheric conditions. Thériault et al. (2012) and Colli et al. (2015c) showed that the shape of the snowflake size distribution could influence the collection efficiency.

d. Dataset

In addition to the numerical simulations, the results were compared with observations. Figure 2 shows the location and orientation of the DFIRs at the Marshall site. The same type of instrument (Geonor T-200B) is used to measure the amount of solid precipitation in both DFIRs. The DFIRs were installed upstream of the

other weather instruments, which is on the north of the site because of the northerly prevailing winds. Thus the wind flow is not disturbed upstream of the fence. According to Fig. 2, the SDFIR corresponds to a 0° orientation while the NDFIR corresponds to a 22.5° orientation with respect to north. This is the ideal orientation to study the impact of wind direction on the DFIR collection efficiency.

The temperature, wind speed and direction, and precipitation rate measured by the two DFIRs during the winters of 2012–14 were used in this study. Note that the 3-m tower wind data have been chosen for this study because they are the wind speed and direction at the height of the orifice of the gauge. The 30-min average of the precipitation rate measured by the two DFIRs, the wind speed, and the temperature was used. The wind direction was divided into 90 bins of 4° intervals. Then the mode over 30 min was used as the mean wind direction during that time sample. To differentiate the type of snow, it was assumed that dry snow is associated with temperatures below -4°C and that wet snow occurs between -4° and -0.5°C following the assumption that was made in Thériault et al. (2012). Wet snowflakes occur at warm temperatures, whereas dry snowflakes occur at colder temperature. It is well known in the field of cloud physics that ice is stickier at temperatures of $> -4^\circ$ (Pruppacher and Klett 1997). In addition, snow at temperatures of $> -4^\circ\text{C}$ tends to have a higher density because of partial melting and riming (Rogers 1974). Therefore, we assumed that wet snowflakes are denser than dry snow, with different terminal velocities as given by Rasmussen et al. (1999). The upper temperature of -0.5°C was chosen to make sure that only solid precipitation is used in this study.

The collection ratio of the two DFIRs was computed by comparing the 30-min-average precipitation rate of the south DFIR with the 30-min average of the precipitation from the north DFIR:

$$\text{CR} = R_{\text{SDFIR}}/R_{\text{NDFIR}}, \quad (9)$$

where R_{SDFIR} and R_{NDFIR} are the precipitation rates measured by the Geonor T-200B gauge placed in the south and north DFIRs, respectively. The sample was chosen to have an average precipitation rates of greater than 0.5 mm h^{-1} for both gauge–shield configurations. The data were further chosen to have a wind direction at 3 m ranging over $\pm 15^\circ$ around north.

3. Flow field analysis

To study the collection efficiency of the DFIR, it is essential to assess the behavior of the flow field for the

two wind directions. The streamlines on a horizontal plane at various heights as well on a vertical cross section passing through the center of the DFIR are examined, as is the vertical motion above the center of the gauge.

Figure 3 compares the streamlines for the two DFIR orientations at different heights of 4, 3.5, and 3 m above ground. Note that the top of the gauge is at 3 m. Note also that the 0° flow-field orientation is associated with converging streamlines inside the inner fence, whereas the 22.5° flow field produces straight streamlines (Figs. 3a,b). Second, the streamlines at the height of the outer fence (Figs. 3c,d) show some significant divergence (0°) within the DFIR, whereas the 22.5° flow field has less divergence. The streamlines provide insight on the trajectory that the snowflake will have when entering the DFIR from different orientations of the vertex. For example, a slow-falling snowflake tends to follow the streamlines more than does a fast-falling one. Therefore, if the flow field converges near the gauge height (Figs. 3e,f), the snowflake trajectories will tend to converge, leading to a higher collection efficiency when compared with a snowflake falling within a diverging flow field.

Because snowflakes tend to follow streamlines, it is useful to look at the vertical cross section of streamlines. Figure 4 shows a vertical cross section parallel to the initial wind speed for the two DFIR orientations. Notice that, in general, the streamlines are associated with an upward motion upstream of the outer fence and have a completely different behavior when entering the DFIR. For example, the 0° DFIR orientation has an impact on the streamlines, which tend to converge in the vertical plane near the vicinity of the gauge. On the other hand, the fence blocks the wind speed entering the DFIR oriented at 22.5° . In this case there is a considerable decrease of the wind speed inside the DFIR relative to the 0° one.

The collection efficiency depends strongly on the strength of vertical motion just above the gauge. Figure 5 shows the vertical profile of the vertical velocity above the center of the gauge. The vertical velocity varies over $\pm 1 \text{ m s}^{-1}$ depending on the orientation of the DFIR and the wind speed. The airflow is downward for the wind orientation coming from 0° , whereas the vertical velocity is upward for 22.5° . The strength of the flow field above the gauge is also much lower for the 22.5° orientation than for 0° : the absolute value is lower by nearly a factor of 2 for the 22.5° when compared with that for 0° . This flow field suggested that the 0° wind orientation leads to convergence of the flow above the gauge, whereas divergence is associated with 22.5° at the same location. This agrees well with the streamlines presented in Fig. 4.

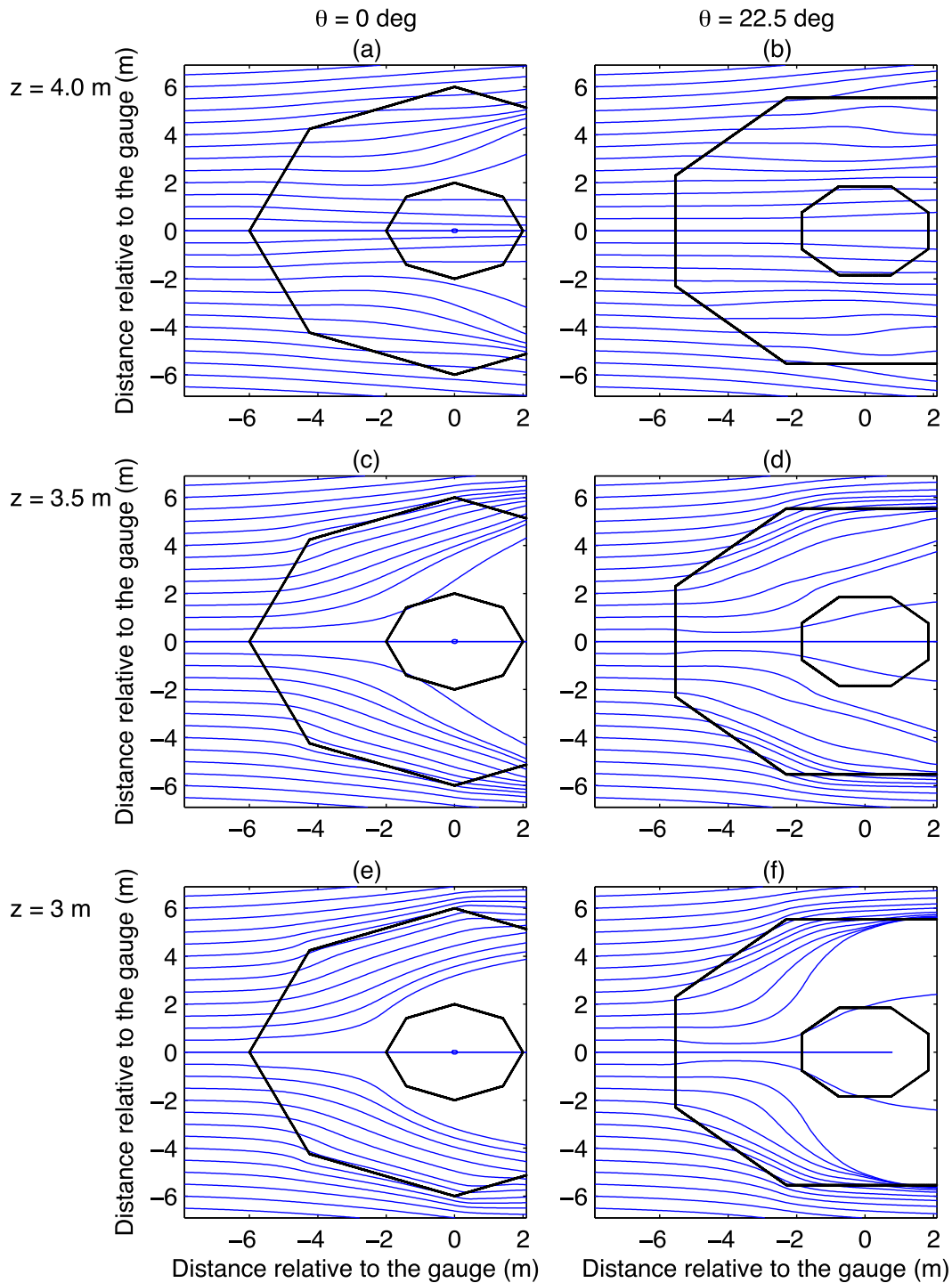


FIG. 3. Flow field at three heights above the ground [(a),(b) 4, (c),(d) 3.5, and (e),(f) 3 m] for a 5 m s^{-1} wind speed associated with the (left) 0° and (right) 22.5° DFIR orientations.

4. Theoretical catch efficiency

To compute the collection efficiency of the DFIR, the trajectory of snowflakes was calculated. Depending on

the flow field and the type of snowflake, the trajectories vary and affect the collection efficiency. Figure 4 shows the difference in the trajectories for the same snowflake type and size associated with two orientations of the

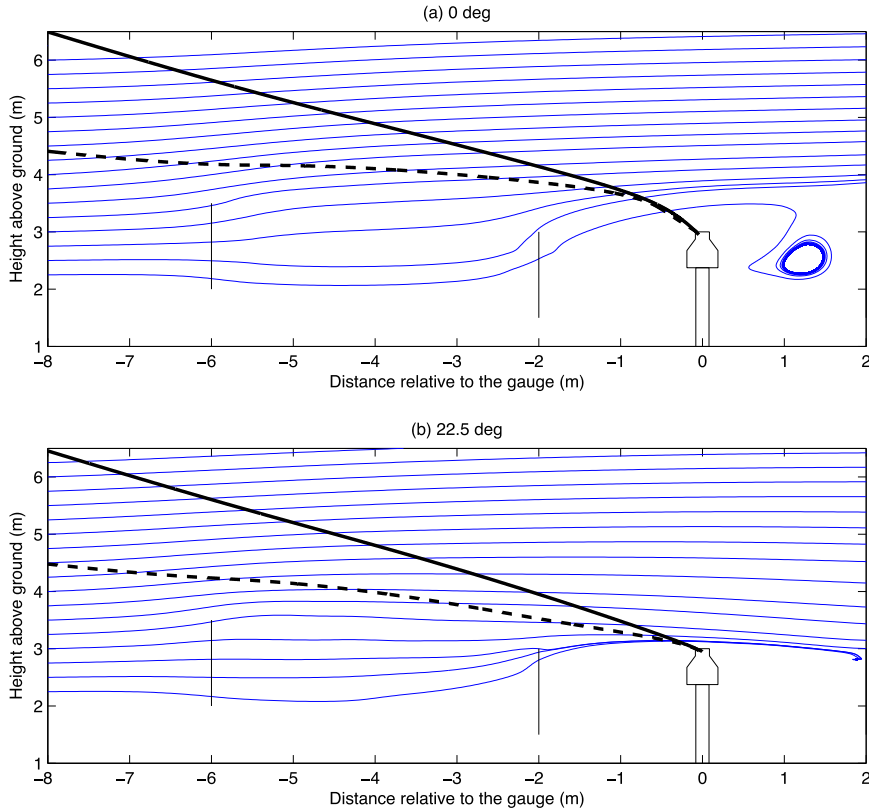


FIG. 4. Flow field (blue lines) at $y = 0$ for the 5 m s^{-1} wind speed (a) 0° and (b) 22.5° . The black lines are the trajectories of wet (solid line) and dry (dashed line) snow of 1-mm diameter. The thin black lines are the DFIR and the precipitation gauge.

DFIR. The trajectories vary for different DFIR orientations because the flow field inside the DFIR varies with its orientation. For instance, when the wind blows perpendicular to a side of the DFIR (22.5°), it slows down the snowflakes entering the fence, and this allows the particles to fall straight into the gauge. On the other hand, when the wind blows on a vertex, the trajectory of the same snowflake will differ because the flow field converges near the gauge height in the center of the DFIR. This causes the snowflake to fall toward the gauge orifice more gradually than for the 0° flow field. For the wet snow particles, the trajectories are somewhat different because, for the same given size, wet snow generally falls faster than dry snow and often crosses the streamlines.

Because the trajectories of the different sizes of snowflakes differ, we expect that the size distribution of snow falling inside the DFIR would be different than the actual one. Figure 6 shows the size distribution of wet and dry snow falling in the gauge with respect to the 0° and 22.5° DFIR orientations. The collection efficiency of dry snow is generally more variable than that for wet snow. For example, the collection efficiency associated

with the vertex flow field is greater than 300% for smaller dry snowflakes and decreases as the snowflakes size increases (Fig. 6a). On the other hand, the collection efficiency associated with the flow perpendicular to a

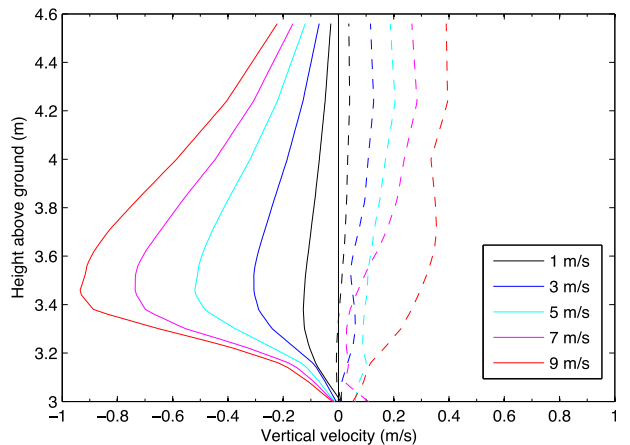


FIG. 5. Vertical motion above the gauge for 1, 3, 5, 7, and 9 m s^{-1} initial horizontal wind speed at 0° (solid lines) and 22.5° (dashed lines).

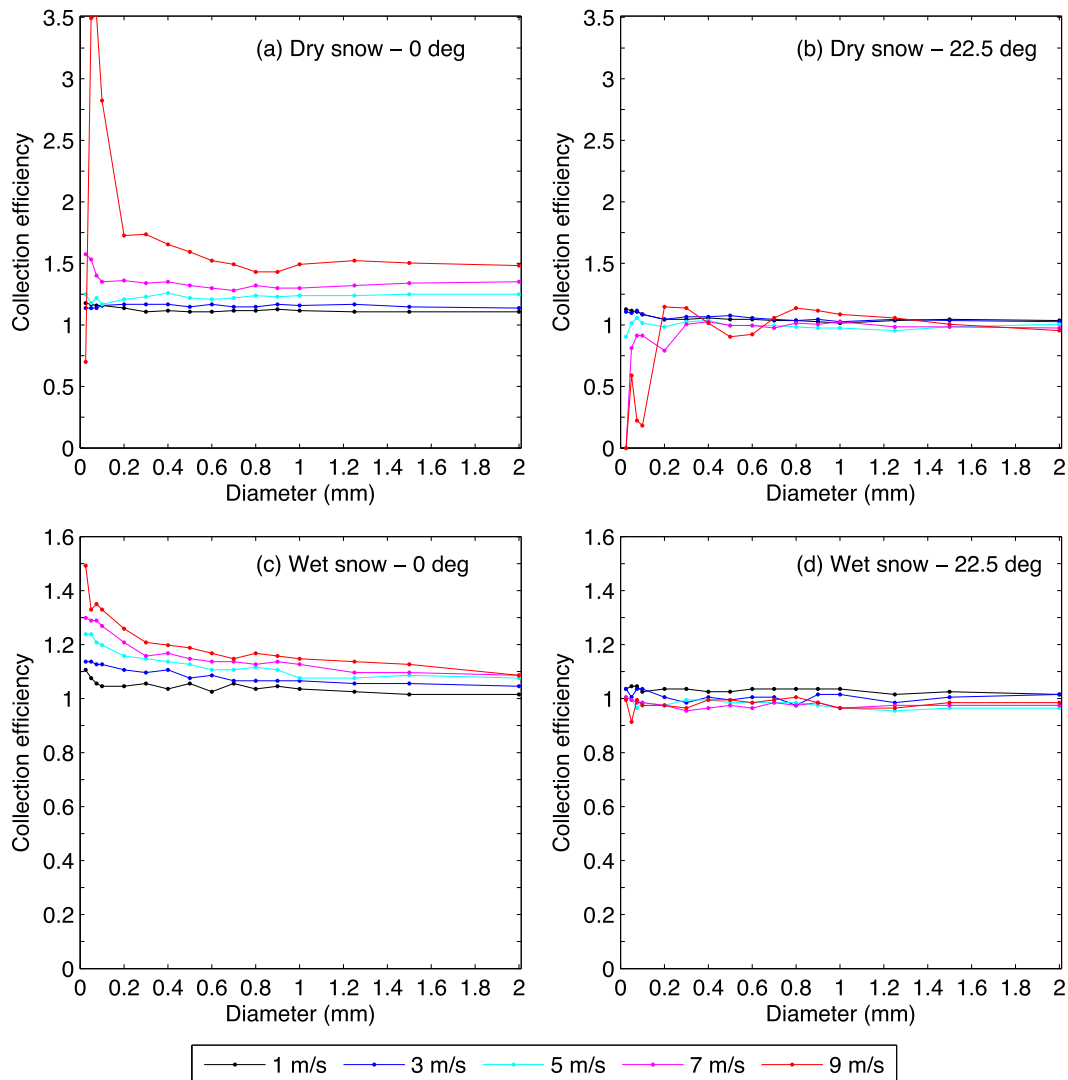


FIG. 6. The collection efficiency of each snowflake type [(a),(b) dry and (c),(d) wet snow] and size for the two wind orientations [(left) 0° and (right) 22.5°] and the five wind speeds (1, 3, 5, 7, and 9 m s^{-1}) that were tested.

side of the DFIR is less than 100% and increases to near 100% with increasing snowflake diameter (Fig. 6b). This behavior is mainly obtained when wind speed $\geq 7 \text{ m s}^{-1}$. The difference in the collection efficiency for different wind orientations is due to the different flow-field behaviors in the vicinity of the gauge. For the 0° orientation, more dry snowflakes will fall into the gauge than will in still air because of the convergence of the streamlines at heights higher than the outer fence (Figs. 3a,b). Slow-falling snowflakes such as dry snow tend to follow the streamlines; hence, their trajectories will converge. On the other hand, because wet snow falls faster than dry snow, they tend to cross more the streamlines, which lead to a collection efficiency that is closer to 100%. The collection efficiency of a small wet

snowflake can reach up to 150% for the 0° DFIR orientation (Fig. 6c), which was a similar trend for dry snow for the same DFIR orientation because of the converging streamlines. For the flow field perpendicular to a side of the DFIR (22.5°), wet snow has a collection efficiency of 100% for all diameters (Fig. 6d) and wind speeds. According to these theoretical results, one could suppose that the flow field within $\sim 1 \text{ m}$ of the inner fence of the DFIR has the most influence on the trajectory of the particle (cf. Fig. 4).

The variation in the trajectories and the size distributions is directly linked to the collection of snow by the gauge. The collection efficiency was calculated by using Eq. (8) for each horizontal wind speed studied, and the results are depicted in Fig. 7. In general, the collection

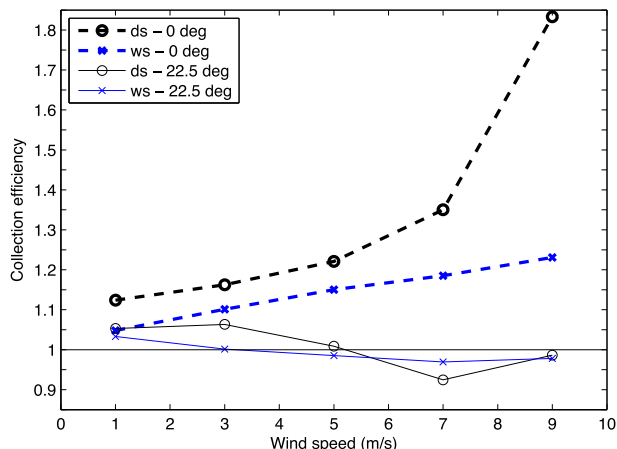


FIG. 7. Theoretical collection efficiency vs wind speed, computed for dry (ds) and wet (ws) snow for the two DFIR orientations (0° and 22.5°). The collection efficiency was computed with Eq. (7) and using a slope parameter $\lambda = 1 \text{ mm}^{-1}$.

efficiency of all types of snow varies with the orientation of the DFIR and the type of snow. The collection efficiency associated with the 0° DFIR orientation is higher than that for the 22.5° one. The 22.5° DFIR orientation is generally associated with diverging horizontal flow field above the gauge because of the blocked wind flow on the side of the DFIR. This causes the collection efficiency to decrease with increasing wind speed. On the other hand, the converging streamlines above the gauge, which were produced by the flow coming on a vertex of the DFIR, lead to increasing collection efficiency with wind speed for both types of snow because of the converging flow field.

The collection efficiency is between 100% and 120% for all cases at wind speeds of $<4 \text{ m s}^{-1}$. At stronger wind speeds, the orientation of the DFIR has a large effect on the collection efficiency, particularly for dry snow. Even if the collection efficiency of wet snow increases with increasing wind speed for the 0° DFIR orientation, it reaches a maximum of 120% at 9 m s^{-1} , whereas dry snow reaches 190% for the same wind speed and DFIR orientation.

Only one value of the slope parameter λ of the snow size distribution was used. Given the variation of the collection efficiency of a given snowflake size, the overall collection efficiency would be affected by the slope of the size distribution. For example, a steeper slope (higher value of λ) leads a lower concentration of large snowflakes, and therefore, for a given wind direction, the collection efficiency would change. According to Fig. 6, a larger value of λ would lead to higher collection efficiency for dry snow (0°), whereas this would probably have no impact on the collection

efficiency of wet snow interacting with a 22.5° DFIR orientation.

5. Comparison with observations

The theoretical results have been compared with observations collected at the Marshall site. The data that were used in comparisons with the theoretical results come from two DFIRs with a Geonor T-200B gauge installed at the center. During precipitation, there were no significant obstacles to the flow from the predominant flow directions, which span from northerly to southeasterly (Fig. 2). One of the DFIRs is located farther north (NDFIR) than the other one (SDFIR). Note that the SDFIR and the NDFIR correspond to the simulated 0° and 22.5° DFIR orientations, respectively. In other words, a northerly wind at the Marshall test site is associated with the wind flow coming onto a vertex of the SDFIR, which corresponds to the simulated 0° orientation. Therefore, the ratio of precipitation rates measured by the SDFIR and NDFIR (called collection ratio) have been calculated for wind speeds coming from $\pm 15^\circ$ with respect to north to study variations of collection on the basis of wind direction relative to the geometry of the DFIR.

To compare the results with observations, the collection ratio of the precipitation rates measured by the SDFIR and the NDFIR [Eq. (9)] is given in Fig. 8. The collection ratio is shown as a function of wind speeds measured by the 3-m tower (gauge height). Much scatter is observed in the data, but the median of the collection ratio increases with increasing wind speed. For example, 50% of the data for wind speeds up to 6 m s^{-1} are between 100% and 120%. The median collection ratio is near 100% at wind speeds up to 3 m s^{-1} , and it starts increasing up to 140% at 7 m s^{-1} . The variability of these data confirms the theoretical prediction that the amount of snow in the DFIR will depend on the wind direction impacting the octagonal shape of the DFIR.

The data have been divided into wet and dry snow to investigate the impact of the type of snow on the collection efficiency of the DFIR (Figs. 9a,b). Dry snow is defined as solid precipitation falling at temperatures of $<-4^\circ\text{C}$, and wet snow is solid precipitation falling at temperatures between -4° and -0.5°C . The results show the impact of crystal type and the orientation of the DFIR on the collection efficiency.

The ratio associated with dry snow shows the SDFIR collecting more snow as the wind speed increases. The mean value is near 160% for dry snow at 7 m s^{-1} , and the results are similar to the theoretical calculations. The ratio measured by the DFIRs for wet snow shows a smaller increase with wind speed than is observed for

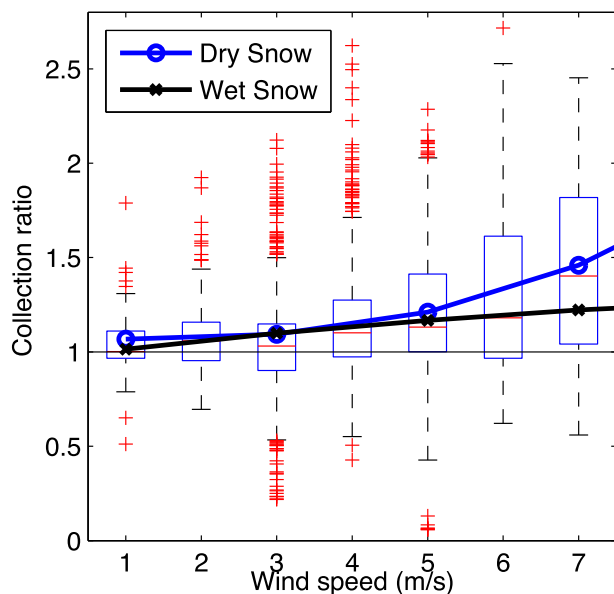


FIG. 8. The theoretical collection efficiency for wet (thick black line) and dry (thick blue line) snow in comparison with the observations (box plots) for winters 2012/13 and 2013/14. The 3-m tower wind speed and direction were used. The collection ratio (SDFIR/NDFIR) is given as the ratio of the precipitation measured by the SDFIR (0°) with respect to the NDFIR (22.5°).

dry snow. The above results are consistent with the theoretical calculation that the ratio associated with the SDFIR should increase with increasing wind speed with respect to the NDFIR, with a stronger increase for dry snow. Note that the theoretical results remain within the whiskers of the box plots.

These results identified sources of uncertainty in DFIR measurements that are associated with the wind speed and direction as well as snow type. A number of them should be noted. We assumed that the dry snow fell more slowly than wet snow, and the only criterion differentiating the type of snow here is the temperature. It is possible that heavily rimed particles occur at a temperature of $< -4^\circ\text{C}$, which would affect the collection efficiency because they fall faster than dry snow. Depending on the wind direction, it can increase (0°) or decrease (22.5°) the collection efficiency. The simulations did not include a single Alter shield placed in the middle of the DFIR. However, the data collected by the precipitation-shield configuration in the field had a single Alter shield. This shield can lead to turbulence and thus can influence the collection efficiency (Colli et al. 2015b). The simulations showed that most of the precipitation that enters the gauge in the middle of the double fence comes from above the fences. Therefore, it does not interact with the flow field near the top of the single Alter shield as it would for a single Alter shield

that is not surrounded by a double fence. This result could be investigated in a further study. It is also possible that the flow field that is perturbed by the NDFIR affects the flow field of the SDFIR because it is located slightly downstream of it. Also, the precipitation rate measured can vary depending on the time average used, the quality of the sensor, use of a heated orifice, or other technical aspects.

6. Concluding remarks

Numerical simulations associated with the Double Fence Intercomparison Reference were performed to assess the measurement of precipitation in that type of shield as a function of wind direction and snow type. In this study, the DFIR refers to the double fence with only a Geonor T-200B gauge. A similar configuration with the addition of a single Alter shield around the Geonor T-200B is currently used as the WMO SPICE reference for the automated snow gauge (Nitu et al. 2012). The CFD approach in combination with a Lagrangian model was used to compute theoretical collection efficiencies.

Because the DFIR is octagonal, two DFIR orientations have been studied. Our findings showed that two mechanisms have an impact on the snow trajectories:

- 1) When the flow-field direction is onto a vertex, the airflow produced by the DFIR converges near the top of the gauge.
- 2) When the flow-field direction is onto a flat side of the DFIR, the airflow produced by the DFIR is blocked.

These mechanisms influenced the overall collection efficiency of the DFIR.

The collection efficiency associated with wind impacting the vertex of the DFIR is higher than flow impacting the sidewall because of the convergence of the flow field near the center of the DFIR. Slow-falling snowflakes tend to follow the streamlines, which in the case of converging streamlines will cause the collection efficiency to be greater than 100% in some instances. On the other hand, wet snow generally crosses the streamlines, which produces a collection efficiency of $100 \pm 20\%$ for any wind speed. Also, the theoretical collection efficiency would vary with the slope of the snow size distribution. For example, a flatter slope would lead to a higher collection efficiency of dry snow. On the other hand, no major differences would be observed in the wet-snow collection efficiency.

The theoretical results were compared with observations collected by differently oriented DFIRs at the Marshall test site. For a northerly wind, the SDFIR is

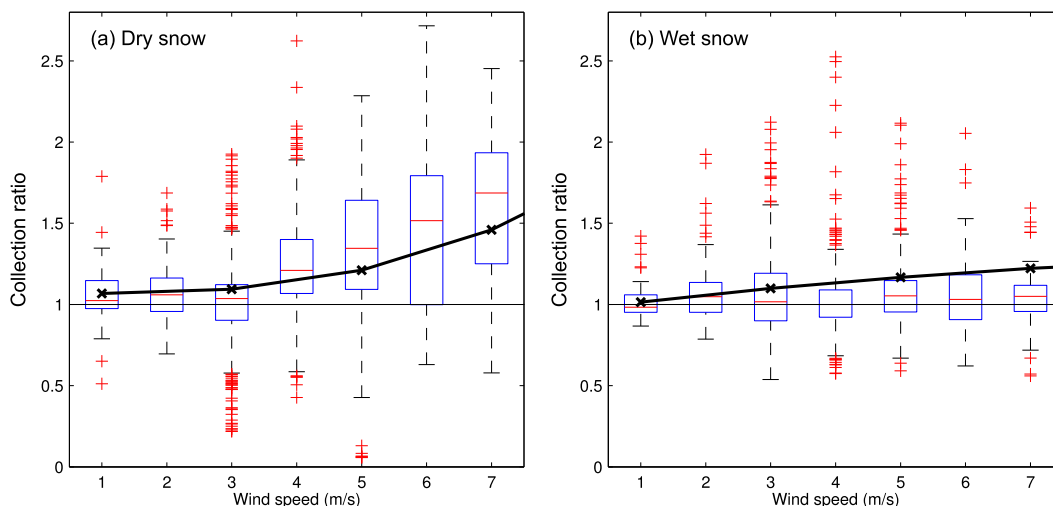


FIG. 9. Comparison of the theoretical collection efficiency (solid black line) with the observations (box plots) for (a) dry snow and (b) wet snow. Dry snow is associated with temperatures of less than -4°C , and wet snow is associated with temperatures between -0.5° and -4°C .

oriented as the theoretical 0° orientation, whereas the NDFIR is oriented as the theoretical 22.5° . The collection ratio of both DFIRs was compared for wind speeds (3-m tower) coming from $\pm 15^{\circ}$ around north over a 2-yr period. The results showed that for dry snow conditions the SDFIR collects more snow as wind speed increases, whereas the collection ratio associated with wet snow remains generally constant with wind speed. The results were comparable to the numerical-modeling results. Therefore, the wind speed and direction as well as the type of snow affect the amount of precipitation that is measured by the DFIR.

Further investigation of the characteristics of the DFIR should be conducted. The collection efficiency associated with a circular DFIR and whether or not the inner fence is needed should be studied. The results suggest that the main factor that affects precipitation amount is the orientation of the outer fence with respect to the wind direction. Also, the 22.5° orientation leads to convergence of the flow near the center of the fence. It would be worth testing the collection efficiency of the smaller version of DFIR that is also installed at the Marshall test site. The impact of the single Alter shield placed in a DFIR should also be considered. The movement of the slats leads to a disturbance of the flow that could affect the number of snowflakes that fall in the gauge. If no significant impact was found from these tests, it may be possible to simplify the geometry and construction of a DFIR.

Overall, this study demonstrated that the WMO second reference for solid precipitation often overcollects solid precipitation as the wind speed increases, depending on wind direction and snow type. This result

should be taken into account when using the DFIR to develop transfer functions for the various snow gauge-wind shield systems that are currently manufactured.

Acknowledgments. This research was funded by the Natural Sciences and Engineering Research Council of Canada. Andy Gaydos and Scott Landolt (NCAR) provided the data used to compare the theoretical results. A special thank you is given to Jeffery Hoover and Rodica Nitu (Environment Canada) for providing an initial version of the DFIR geometry for the CFD simulations. Roy Rasmussen acknowledges support of the NCAR Water System program funded by the National Science Foundation.

REFERENCES

- Alter, J. C., 1937: Shielded storage precipitation gauges. *Mon. Wea. Rev.*, **65**, 262–265, doi:[10.1175/1520-0493\(1937\)65<262:SSPG>2.0.CO;2](https://doi.org/10.1175/1520-0493(1937)65<262:SSPG>2.0.CO;2).
- Colli, M., L. G. Lanza, R. Rasmussen, and J. M. Thériault, 2015a: The collection efficiency of shielded and unshielded precipitation gauges. Part I: CFD airflow modeling. *J. Hydrometeorol.*, doi:[10.1175/JHM-D-15-0010.1](https://doi.org/10.1175/JHM-D-15-0010.1), in press.
- , —, —, and —, 2015b: The collection efficiency of shielded and unshielded precipitation gauges. Part II: Modeling particle trajectories. *J. Hydrometeorol.*, doi:[10.1175/JHM-D-15-0011.1](https://doi.org/10.1175/JHM-D-15-0011.1), in press.
- , R. Rasmussen, J. M. Thériault, L. G. Lanza, C. B. Baker, and J. Kochendorfer, 2015c: An improved trajectory model to evaluate the collection performance of snow gauges. *J. Appl. Meteor. Climatol.*, **54**, 1826–1836, doi:[10.1175/JAMC-D-15-0035.1](https://doi.org/10.1175/JAMC-D-15-0035.1).
- Goodison, B. E., P. Y. T. Louie, and D. Yang, 1998: WMO solid precipitation measurement intercomparison. Instruments and Observing Methods Rep. No. 67 and WMO/TD No. 872, 318 pp. [Available online at <http://www.wmo.int/pages/prog/www/reports/WMOtd872.pdf>.]

- Groisman, P. Ya., and D. R. Legates, 1994: The accuracy of United States precipitation data. *Bull. Amer. Meteor. Soc.*, **75**, 215–227, doi:[10.1175/1520-0477\(1994\)075<0215:TAO USP>2.0.CO;2](https://doi.org/10.1175/1520-0477(1994)075<0215:TAO USP>2.0.CO;2).
- , V. V. Koknaeva, T. A. Belokrylova, and T. R. Karl, 1991: Overcoming biases of precipitation measurement: A history of the USSR experience. *Bull. Amer. Meteor. Soc.*, **72**, 1725–1733, doi:[10.1175/1520-0477\(1991\)072<1725:OBOPMA>2.0.CO;2](https://doi.org/10.1175/1520-0477(1991)072<1725:OBOPMA>2.0.CO;2).
- Houze, R. A., P. V. Hobbs, and P. H. Herzegh, 1979: Size distributions of precipitation particles in frontal clouds. *J. Atmos. Sci.*, **36**, 156–162, doi:[10.1175/1520-0469\(1979\)036<0156:SDOPPI>2.0.CO;2](https://doi.org/10.1175/1520-0469(1979)036<0156:SDOPPI>2.0.CO;2).
- Khvorostyanov, V., and J. Curry, 2005: Fall velocities of hydrometeors in the atmosphere: Refinements to a continuous analytical power law. *J. Atmos. Sci.*, **62**, 4343–4357, doi:[10.1175/JAS3622.1](https://doi.org/10.1175/JAS3622.1).
- Marshall, J. S., and W. M. Palmer, 1948: The distribution of raindrops with size. *J. Meteor.*, **5**, 165–166, doi:[10.1175/1520-0469\(1948\)005<0165:TDORWS>2.0.CO;2](https://doi.org/10.1175/1520-0469(1948)005<0165:TDORWS>2.0.CO;2).
- Nespor, V., and B. Sevruc, 1999: Estimation of wind-induced error of rainfall gauge measurements using a numerical simulation. *J. Atmos. Oceanic Technol.*, **16**, 450–464, doi:[10.1175/1520-0426\(1999\)016<0450:EOWIEO>2.0.CO;2](https://doi.org/10.1175/1520-0426(1999)016<0450:EOWIEO>2.0.CO;2).
- Nitu, R., and Coauthors, 2012: WMO intercomparison of instruments and methods for the measurement of solid precipitation and snow on the ground: Organization of the experiment. Preprints, *TECO-2012: WMO Technical Conf. on Meteorological and Environmental Instruments and Methods of Observations*, Brussels, Belgium, WMO, 10 pp. [Available online at https://www.wmo.int/pages/prog/www/IMOP/publications/IOM-109_TECO-2012/Session1/O1_01_Nitu_SPICE.pdf.]
- Pruppacher, H. R., and J. D. Klett, 1997: *Microphysics of Clouds and Precipitation*. 2nd ed. Kluwer Academic Publishers, 954 pp.
- Rasmussen, R. M., J. Vivekanandan, J. Cole, B. Meyers, and C. Masters, 1999: The estimation of snowfall rate using visibility. *J. Appl. Meteor.*, **38**, 1542–1563, doi:[10.1175/1520-0450\(1999\)038<1542:TEOSRU>2.0.CO;2](https://doi.org/10.1175/1520-0450(1999)038<1542:TEOSRU>2.0.CO;2).
- , and Coauthors, 2001: Weather support to deicing decision making WSDDM: A winter weather nowcasting system. *Bull. Amer. Meteor. Soc.*, **82**, 579–595, doi:[10.1175/1520-0477\(2001\)082<0579:WSTDDM>2.3.CO;2](https://doi.org/10.1175/1520-0477(2001)082<0579:WSTDDM>2.3.CO;2).
- , and Coauthors, 2012: How well are we measuring snow: The NOAA/FAA/NCAR winter precipitation test bed. *Bull. Amer. Meteor. Soc.*, **93**, 811–829, doi:[10.1175/BAMS-D-11-00052.1](https://doi.org/10.1175/BAMS-D-11-00052.1).
- Rogers, D. C., 1974: The aggregation of natural ice crystals. M.S. thesis, Dept. of Atmospheric Resources, College of Engineering, University of Wyoming, 91 pp.
- Smith, C., 2009: The relationship between snowfall catch efficiency and wind speed for the Geonor T-200B precipitation gauge utilizing various wind shield configurations. *Proc. 77th Western Snow Conf.*, Canmore, AB, Canada, 115–221.
- Sugiura, K., T. Ohata, and D. Yang, 2006: Catch characteristics of precipitation gauges in high-latitude regions with high winds. *J. Hydrometeorol.*, **7**, 984–994, doi:[10.1175/JHM542.1](https://doi.org/10.1175/JHM542.1).
- Thériault, J. M., R. Rasmussen, K. Ikeda, and S. Landolt, 2012: Dependence of snow gauge collection efficiency on snowflake characteristics. *J. Appl. Meteor. Climatol.*, **51**, 745–762, doi:[10.1175/JAMC-D-11-0116.1](https://doi.org/10.1175/JAMC-D-11-0116.1).
- Yang, D., 2014: Double fence intercomparison reference (DFIR) vs. bush gauge for “true” snowfall measurement. *J. Hydrol.*, **509**, 94–100, doi:[10.1016/j.jhydrol.2013.08.052](https://doi.org/10.1016/j.jhydrol.2013.08.052).
- , and Coauthors, 1995: Accuracy of Tretyakov precipitation gauge: Result of WMO intercomparison. *Hydrol. Processes*, **9**, 877–895, doi:[10.1002/hyp.3360090805](https://doi.org/10.1002/hyp.3360090805).
- , D. Kane, Z. Zhang, D. Legates, and B. Goodison, 2005: Bias corrections of long-term (1973–2004) daily precipitation data over the northern regions. *Geophys. Res. Lett.*, **32**, L19501, doi:[10.1029/2005GL024057](https://doi.org/10.1029/2005GL024057).

Copyright of Journal of Applied Meteorology & Climatology is the property of American Meteorological Society and its content may not be copied or emailed to multiple sites or posted to a listserv without the copyright holder's express written permission. However, users may print, download, or email articles for individual use.